

Electronic Supplmenatry Information

Alumina supported highly dispersed platinum-copper nanocatalyst
with good dehydrogenation performance for
perhydromonobenzyltoluene as a hydrogen carrier

Qiuyue Ding,¹ Yixuan Zhang,² Huijie Wei,² Qing Li,² Yanyan Xi,³ Songqing Hu,^{1} Xufeng
Lin^{2,4*}*

¹College of Material Science and Engineering, China University of Petroleum (East
China), Qingdao, P. R. China, 266580

²College of Chemistry and Chemical Engineering, China University of Petroleum (East
China), Qingdao, P. R. China, 266580

³Advanced Chemical Engineering and Energy Materials Research Center, China
University of Petroleum (East China), Qingdao, P. R. China, 266580

⁴State Key Laboratory of Heavy Oil Processing, China University of Petroleum (East
China), Qingdao, P. R. China, 266580

1. Catalyst characterization for basic physiochemical properties

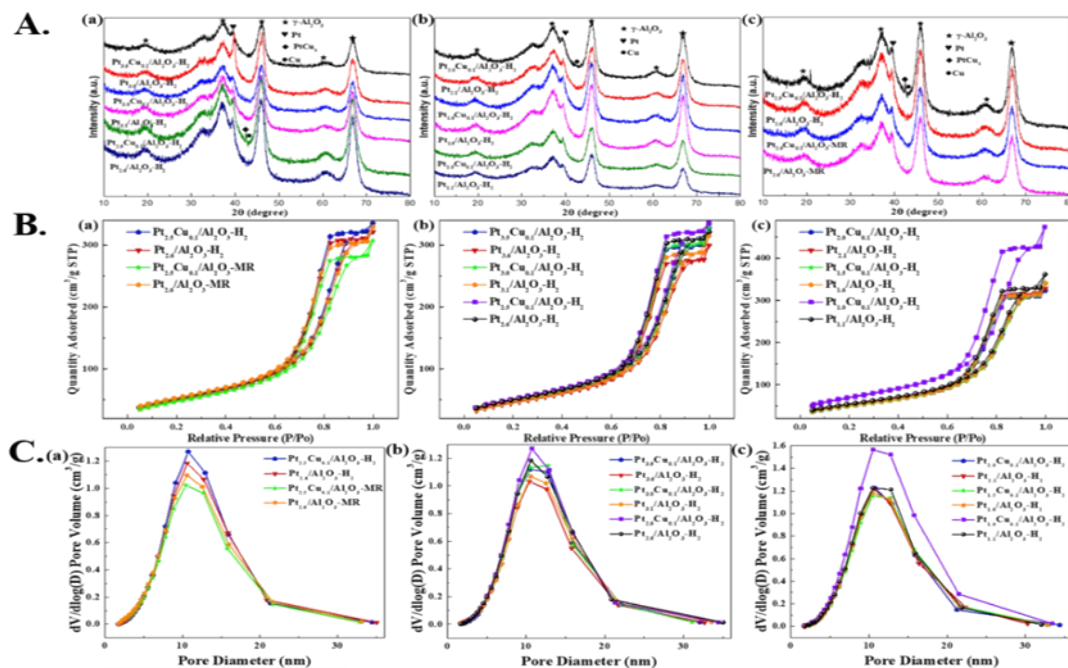


Figure S1. A) Powder XRD patterns of Pt-Cu/Al₂O₃ and Pt/Al₂O₃ catalyst powders with different preparation methods and different loading loads; B) N₂ adsorption-desorption isotherms of the prepared Pt-Cu/Al₂O₃ and Pt/Al₂O₃ catalysts; and C) Maximum Pore Size distribution of the prepared Pt-Cu/Al₂O₃ and Pt/Al₂O₃ catalysts.

As shown in Figure S1A, it could be perceived that the XRD spectra of 14 types of Pt and Pt Cu alumina catalysts under different loading amounts and preparation methods have similar characteristics. Especially the sharp peak shapes of the support signified the peaks of 2 θ = 18.8, 36.9, 45.9, 60.5 and 66.8° corresponded to typical characteristic peaks of γ -Al₂O₃. And Pt in the patterns signified the diffraction peak of 2 θ = 39.5° corresponded to and metallic Pt(111) crystal phase. These demonstrated satisfactory crystallinity and dispersion in the Pt component. And it could be seen that the diffraction peak size of metal Pt was decreased with the addition of metal Cu. It indicated that the dispersion of metal Pt in the catalyst could be promoted by the addition of metal Cu. In consequence, the preparation of

the precious metal catalyst with Cu added in this experiment was relatively triumphant. Nevertheless, the small addition of Cu had different impacts on catalysts with different preparation methods and loading amounts. The weak Cu (111) characteristic diffraction peak of $2\theta = 43.3^\circ$ and the 42.4° diffraction peak symbolized the Pt and Cu new phase. And it was consistent with the TEM image in the unique $\text{Pt}_{2.5}\text{Cu}_{0.1}/\text{Al}_2\text{O}_3\text{-H}_2$ catalyst. This explicated the successful formation of Pt-Cu bimetallic alloy and the relationship between the formation of Pt-Cu alloy and the preparation method and loading amount.^{1,2} In contrast, only a small portion of Pt-Cu/ Al_2O_3 catalysts with different loading amounts or preparation methods had weak Cu characteristic peaks, implying the absence of alloys. It was not only related to the extremely low loading amount of Cu, but also indirectly proves that Pt and Cu alloys had not been synthesized or were extremely low. Compared with Figure S1B, the presence of the distinctive Pt-Cu alloy structure was essential for enhancing the 12H-MBT dehydrogenation activity of the Pt-Cu catalyst. The electron transfer shown by XPS also corresponded to the phenomenon, which also attested the synergistic catalytic effect between Pt and Cu in the $\text{Pt}_{2.5}\text{Cu}_{0.1}/\text{Al}_2\text{O}_3\text{-H}_2$ catalyst.

The nitrogen adsorption desorption isotherms of fresh catalysts and supports were shown in Figure S1B. The nitrogen adsorption/desorption isotherms were exhibited the IV patterns in the whole Pt-Cu/ Al_2O_3 and Pt/ Al_2O_3 catalysts mentioned, with the existence of H_2 (b) hysteresis loops. As P/P_0 increased, the saturated adsorption platform appeared, explicating that the above catalysts were mainly mesoporous materials with uniform and relatively wide pore size distribution.^{3,4} And the pore size distribution was mostly between 10-13nm. In accordance with the analysis of the pore structure, it could be ascertained that

the mesoporous characteristics were mainly derived from the pore structure of the Al₂O₃ support.

Table S1. Textural properties of the prepared Pt-Cu/Al₂O₃ and Pt/Al₂O₃ catalysts.

Sample	S _{BET} (m ² /g)	V _p (cm ³ /g)	D _{mode} (nm)
Pt _{3.5} Cu _{0.1} /Al ₂ O ₃ -H ₂	178.8	0.47	10.49
Pt _{3.6} /Al ₂ O ₃ -H ₂	165.3	0.43	10.40
Pt _{3.0} Cu _{0.1} /Al ₂ O ₃ -H ₂	178.7	0.47	12.80
Pt _{3.1} /Al ₂ O ₃ -H ₂	170.7	0.45	10.57
Pt _{2.5} Cu _{0.1} /Al ₂ O ₃ -H ₂	187.8	0.50	10.73
Pt _{2.6} /Al ₂ O ₃ -H ₂	182.8	0.48	10.59
Pt _{2.5} Cu _{0.1} /Al ₂ O ₃ -MR	173.9	0.44	10.43
Pt _{2.6} /Al ₂ O ₃ -MR	193.0	0.48	10.57
Pt _{2.0} Cu _{0.1} /Al ₂ O ₃ -H ₂	183.1	0.48	10.74
Pt _{2.1} /Al ₂ O ₃ -H ₂	185.7	0.49	10.54
Pt _{1.5} Cu _{0.1} /Al ₂ O ₃ -H ₂	181.4	0.49	10.44
Pt _{1.6} /Al ₂ O ₃ -H ₂	183.6	0.49	10.42
Pt _{1.0} Cu _{0.1} /Al ₂ O ₃ -H ₂	253.0	0.67	10.48
Pt _{1.1} /Al ₂ O ₃ -H ₂	197.3	0.51	10.48

The pore structure data of the prepared catalyst were listed in Table S1 and Figure S1C. As for the catalysts obtained from H₂ reduction, the specific surface area (S_{BET}), pore volume (V_{p}), and maximum pore size (D_{mode}) were wholly increased to some extent through the addition of copper. At this moment, the platinum loading amount ($\geq 2.5\text{wt}\%$) was higher and the platinum loading amount was the same. It was indicated that the active component was stabilized by calcination after the introduction of Cu under this reduction method. This not only occupied the small internal pores and expanded the pore size, but also emanated to the formation of new pore structures. And it aroused the increase in the latter two and the emergence of the above complex situation, there was no such pattern for catalysts with lower platinum loading ($<2.5\text{wt}\%$). The addition of copper led to the decrease in S_{BET} and the increase in V_{p} , while D_{mode} remains basically unchanged. It was similar to catalysts with lower total loading and smaller metal particles, where several active components were distributed on the catalyst surface and occupied fewer pores. Under such circumstances, it could result in the increase in maximum pore size, the decrease in specific surface area, and the slight variation in pore volume. As far as the extremely low platinum loading ($=1\text{wt}\%$) catalysts were concerned, the proportion of Cu in the overall metal component was large, which had a significant impact. New pore structures appeared more obvious after fixed roasting of the metal components, contributing to a significant increase in S_{BET} and V_{p} . With the addition of copper, S_{BET} , V_{p} and D_{mode} were reduced in the he catalyst (Pt=2.5 wt%) for the key nodes obtained from formaldehyde reduction. Moreover, the S_{BET} of catalyst obtained from formaldehyde reduction was significantly reduced. And the V_{p} and D_{mode} were also smaller compared with the equivalent Pt and Cu loading catalysts obtained from H₂ reduction. It was further

proved that there was the “confinement effect” of $C_{11}H_{16}N_8O_8$ under the liquid-phase reduction method. This made Pt and Cu more dispersed and the formaldehyde reduction reaction more intense. With the result that there might be tiny collapsed pore structures, the pore volume partially decreased and specific surface area diminished. This aroused the phenomenon where the active components occupied partial pores and the pore size decreased. The hydrogen reduction method included calcination fixation of metal components and relatively stable reduction methods. Therefore the specific surface area of $Pt_{2.5}Cu_{0.1}/Al_2O_3-H_2$ catalyst was significantly higher than that of $Pt_{2.5}Cu_{0.1}/Al_2O_3-MR$. Beyond that, the appearance of new pore structures might bring about larger pore volume and pore size. It further described that the metal component dispersion of $Pt_{2.5}Cu_{0.1}/Al_2O_3-H_2$ catalyst was higher. The reason why highly dispersed active components could enhance the catalytic activity of 12H-MBT was that the structure additives was used in the preparation of the catalyst. And this was mainly related to the material and preparation conditions of the catalyst combined with TEM and SEM.

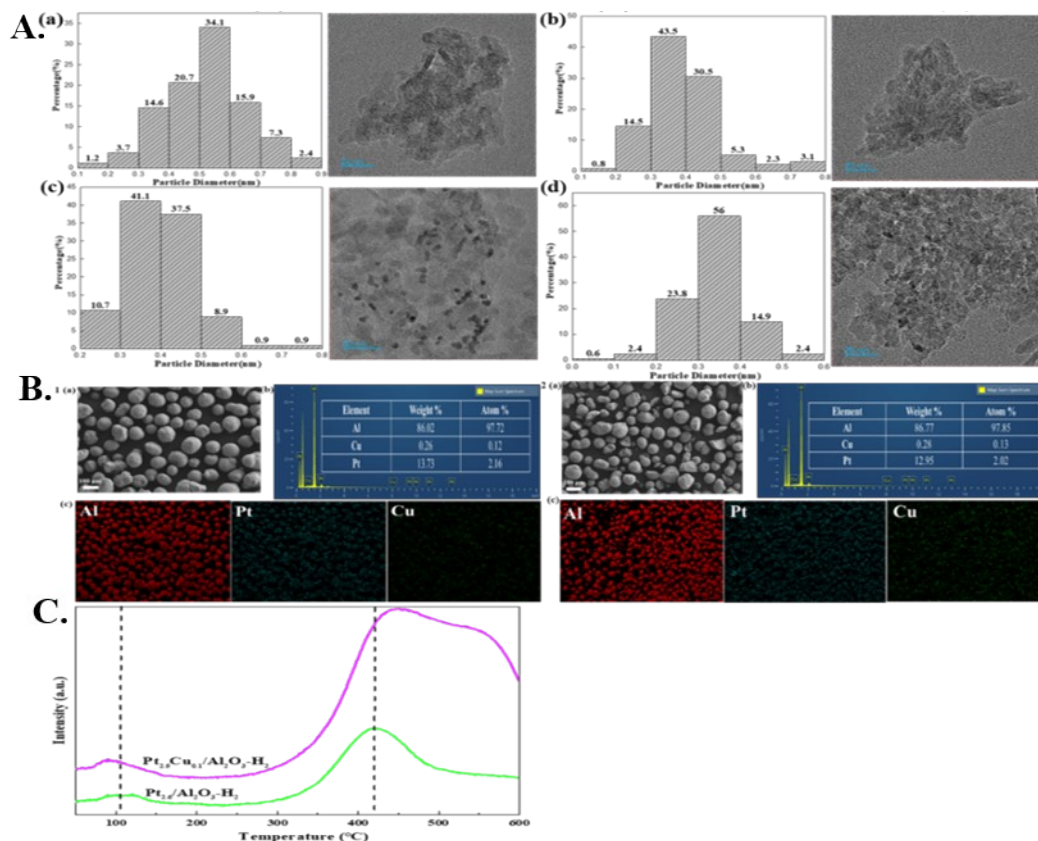


Figure S2. A) The particle size chart and TEM image of (a) $Pt_{2.5}Cu_{0.1}/Al_2O_3-H_2$, (b) $Pt_{2.6}/Al_2O_3-H_2$, (c) $Pt_{2.5}Cu_{0.1}/Al_2O_3-MR$ and (d) $Pt_{2.6}/Al_2O_3-MR$; B) The SEM images and the EDX-mapping for Pt, Cu and Al elements of (1) $Pt_{2.5}Cu_{0.1}/Al_2O_3-H_2$ and (2) $Pt_{2.5}Cu_{0.1}/Al_2O_3-MR$ catalysts and C) H_2 -TPD profiles of $Pt_{2.5}Cu_{0.1}/Al_2O_3-H_2$ and $Pt_{2.6}/Al_2O_3-H_2$ catalysts.

Compared with $Pt_{2.6}/Al_2O_3-H_2$ catalyst, the TEM image (Figure S2A) of $Pt_{2.5}Cu_{0.1}/Al_2O_3-H_2$ catalyst could be observed that Pt grains were highly dispersed on the support. The average particle size of the above catalyst was around 0.52nm, while the average particle size of $Pt_{2.6}/Al_2O_3-H_2$ was around 0.39nm. The occurrence of the above phenomenon was due to the partial formation of alloys (combined with XRD) in the Pt and Cu components. This resulted in larger particle sizes than individual Pt components. Moreover, the addition of Cu and the treatment of Pt and Cu calcination fixation followed

by reduction have the certain anchoring effect on Pt. Therefore, there was no significant aggregation of Pt components under high-temperature reduction. As for the Pt_{2.5}Cu_{0.1}/Al₂O₃-MR catalyst, the average particle size was around 0.40nm, while the average particle size of Pt_{2.6}/Al₂O₃-MR was 0.33nm. Compared with previous studies, it was demonstrated that the confinement effect of imidazolidinylurea was stronger than calcination fixation. And the catalyst obtained by liquid-phase reduction of Cu doped Pt was also highly dispersed and smaller particle size.

In summary, the Pt and Cu catalysts prepared by the two preparation methods had highly dispersed nanoscale metal particle sizes. The particle size prepared by hydrogen reduction was larger than that prepared by formaldehyde reduction. However, their catalytic performance for 12H-MBT dehydrogenation was significantly different. On the one hand, the former preparation method involves the formation of alloy interactions between Pt and Cu, resulting in a better synergistic catalytic effect between Pt and Cu. On the other hand, the reaction substrate molecules were relatively large and can adsorb more catalysts, adsorbing more catalysts active sites. There was no doubt that larger metal particle sizes could better catalyze the reaction substrates in addition to highly dispersed active components. Therefore, individual active sites may be more suitable for practical reactions for this system.

Figure S2B showed that the Pt_{2.5}Cu_{0.1}/Al₂O₃-H₂ catalyst exhibited the distinct spherical morphology, which was the typical Al₂O₃ morphology. This indicated that the introduction of Pt and Cu during the catalyst preparation reduction process didn't significantly alter the support morphology and structure. Compared with the Pt_{2.5}Cu_{0.1}/Al₂O₃-MR catalyst, the morphology of this catalyst was more regular and the actual Pt loading was higher. It

explicated that the hydrogen reduction method after calcination and fixation of Pt and Cu components was more gentle and stable than liquid-phase reduction. And It further indicated that the hydrogen reduction method after calcination and fixation of Pt and Cu components was more gentle and stable than liquid-phase reduction. This made the pore structure relatively stable (corresponding to BET results) and the loss rate of active components smaller, resulting in higher catalytic activity. Furthermore, the distribution of Pt and Cu elements in the two samples was basically consistent with that of Al element in the same region and the distribution of Al element depends on the Al_2O_3 support. It further supported the relatively uniform distribution of Pt and Cu elements on the support surface. Going further, there is also partial overlap in the distribution of Pt and Cu elements in the $\text{Pt}_{2.5}\text{Cu}_{0.1}/\text{Al}_2\text{O}_3\text{-H}_2$ catalyst. This demonstrated the existence of interaction forces between Pt and Cu (XRD, BET, and TEM could confirm this as well)

Adopting H_2 -TPD analysis could investigate the differences in hydrogen species on the surface of $\text{Pt}_{2.5}\text{Cu}_{0.1}/\text{Al}_2\text{O}_3\text{-H}_2$ and $\text{Pt}_{2.6}/\text{Al}_2\text{O}_3\text{-H}_2$ catalysts. This pursued the dehydrogenation active sites of $\text{Pt}_{2.5}\text{Cu}_{0.1}/\text{Al}_2\text{O}_3\text{-H}_2$ catalysts. And it further uncovered the essence of the difference in catalytic performance of Pt for 12H-MBT dehydrogenation reaction with the addition of Cu. As shown in Figure S2C, the H_2 -TPD spectra of $\text{Pt}_{2.5}\text{Cu}_{0.1}/\text{Al}_2\text{O}_3\text{-H}_2$ and $\text{Pt}_{2.6}/\text{Al}_2\text{O}_3\text{-H}_2$ catalysts both exhibited two H_2 desorption peaks. For the above, desorption peaks below $200\text{ }^\circ\text{C}$ were attributed to hydrogen desorption on the metal surface, where chemically adsorbed hydrogen tended to undergo reversible desorption.⁵ However, H_2 desorption peaks above $400\text{ }^\circ\text{C}$ were typically attributed to overflow hydrogen desorption on the support.⁶ In addition, the broad shoulder peak of the first peak originated from hydrogen desorption at the interface between the metal and the

support.⁵ The above comparison found that the hydrogen desorption amount of Pt_{2.5}Cu_{0.1}/Al₂O₃-H₂ from low to high temperature range was significantly higher than that of Pt_{2.6}/Al₂O₃-H₂. This expressed that Pt_{2.5}Cu_{0.1}/Al₂O₃-H₂ catalyst had strong hydrogen overflow or activation ability. The possible reason was that the presence of Pt and Cu alloys weakened the interaction with dissociated hydrogen.^{7,8} This result indicated that the unique alloy structure of Pt_{2.5}Cu_{0.1}/Al₂O₃-H₂ catalyst had the higher hydrogen dissociation or activation ability. This was the primary reason for the high dehydrogenation activity of 12H-MBT.

Table S2. Partial characterization results of the Pt-Cu/Al₂O₃ and Pt/Al₂O₃ catalysts.

sample	Dispersion ^a (%)	metal ^b (wt %)
Pt _{3.5} Cu _{0.1} /Al ₂ O ₃ -H ₂	12.50	3.25
Pt _{3.6} /Al ₂ O ₃ -H ₂	12.59	3.32
Pt _{3.0} Cu _{0.1} /Al ₂ O ₃ -H ₂	15.65	2.89
Pt _{3.1} /Al ₂ O ₃ -H ₂	15.92	2.97
Pt _{2.5} Cu _{0.1} /Al ₂ O ₃ -H ₂	23.53	2.16
Pt _{2.6} /Al ₂ O ₃ -H ₂	23.30	2.48
Pt _{2.5} Cu _{0.1} /Al ₂ O ₃ -MR	23.01	2.02
Pt _{2.6} /Al ₂ O ₃ -MR	23.74	2.32
Pt _{2.0} Cu _{0.1} /Al ₂ O ₃ -H ₂	22.89	1.81
Pt _{2.1} /Al ₂ O ₃ -H ₂	23.01	1.98
Pt _{1.5} Cu _{0.1} /Al ₂ O ₃ -H ₂	30.78	1.48
Pt _{1.6} /Al ₂ O ₃ -H ₂	31.88	1.56
Pt _{1.0} Cu _{0.1} /Al ₂ O ₃ -H ₂	38.09	0.97

Pt_{1.1}/Al₂O₃-H₂ 38.98 1.08

a: Data from CO chemisorption

b: Data from EDX-mapping

Table S2 showed that Pt_{2.5}Cu_{0.1}/Al₂O₃-H₂ catalyst had the higher CO adsorption capacity than Pt_{2.6}/Al₂O₃-H₂ catalyst. This elaborated the higher number of surface hydrogen adsorption active sites, which was the intrinsic reason for its high intrinsic activity (TOF value).

2. Basic data of dehydrogenation reaction test

Table S3. Kinetic data analysis of dehydrogenation of 12H-MBT at different temperatures.

Temperature/ °C	k / mol·s ⁻¹	T / K	$\frac{1}{T}$ / K ⁻¹	lnk / mol·s ⁻¹
220	0.000087	493.15	0.002028	-9.349602
230	0.000145	503.15	0.001987	-8.838777
240	0.000225	513.15	0.001949	-8.399410
250	0.000349	523.15	0.001911	-7.960439
260	0.000478	533.15	0.001876	-7.645900

From Fig. 6 (b) - (f), it showed that the apparent reaction rate constants at the initial stage of dehydrogenation of 12H-MBT from 220 to 260 °C corresponded to k₁, k₂, k₃, k₄, and k₅, respectively. The data of 12H-MBT dehydrogenation reaction at different

temperatures were processed and analyzed, and the obtained data are shown in Table S3. According to the data in Table S3, Ink was plotted against 1/T to acquire a linear fitting line, and the fitting result was shown in Fig. 7a.

References

- 1 Jian C., Zhi-Hui Q., Shuang-Zan LU., and Geng-Yu C, *JCEMS*, 2013.
- 2 Lee J.Y., Han S.B., Kwak D.H., Kim M.C., Lee S., Park J.Y., Choi I.A., Park H.S. and Park K.W, *J. Alloy. Compd.*, 2017, **691**, 26-33.
- 3 Wu Y. S., Ma J., Hu F., and Li, M. C, *JMST*, 2012, **28**(6), 572-576.
- 4 Hong U. G., Hwang S., Seo J. G., Yi J. and Song, I. K, *CATAL LETT*, 2010, **138**, 28-33.
- 5 Cecilia J. A., Infantes-Molina A., Rodríguez-Castellón E. and Jiménez-López A, *J. Catal*, 2009, **263**(1): 4-15.
- 6 Liu X., Chen J. and Zhang J, *IND ENG CHEM RES*, 2008, **47**(15): 5362-5368.
- 7 Zhou L., Yang Y., Chen J., Qiu R. and Yao Y, *SURF SCI*, 2021, **712**, 121892.
- 8 Shen J., Spiewak B. E. and Dumesic J, *Langmuir*, 1997, **13**(10): 2735-2739.